Optics Communications 358 (2016) 169–175

Contents lists available at ScienceDirect

Optics Communications

journal homepage: www.elsevier.com/locate/optcom

Near-field optical thin microcavity theory

Jiu Hui Wu*, Jiejie Hou

School of Mechanical Engineering and State Key Laboratory for Strength and Vibration of Mechanical Structures, Xi'an Jiaotong University, Xi'an 710049, China

ARTICLE INFO

Article history:
Received 17 June 2015
Received in revised form
30 August 2015
Accepted 9 September 2015

Keywords:
Near-field optics
Subwavelength aperture
Edge effect
Depolarization phenomenon

ABSTRACT

The thin microcavity theory for near-field optics is proposed in this study. By applying the power flow theorem and the variable theorem,the bi-harmonic differential governing equation for electromagnetic field of a three-dimensional thin microcavity is derived for the first time. Then by using the Hankel transform, this governing equation is solved exactly and all the electromagnetic components inside and outside the microcavity can be obtained accurately. According to the above theory, the near-field optical diffraction from a subwavelength aperture embedded in a thin conducting film is investigated, and numerical computations are performed to illustrate the edge effect by an enhancement factor of 1.8 and the depolarization phenomenon of the near-field transmission in terms of the distance from the film surface. This thin microcavity theory is verified by the good agreement between our results and those in the previous literatures. The thin microcavity theory presented in the study should be useful in the possible applications of the thin microcavities in near-field optics and thin-film optics.

1. Introduction

Near-field scanning optical microscope (NSOM) is a type of microscope in which a subwavelength aperture at the end of a tapered and aluminum-coated optical fiber is most commonly used as a scanning probe with resolution well beyond the usual "diffraction limit". The probe scans over a surface at a height of a few nanometers above the surface. The understanding of the nature and details of the tip-sample interaction is imperative for quantitative evaluation of near-field images. Since the emergence of NSOM, near-field optics has been developed recently [1–5]. As a simple near-field modeling, the light scattering from a subwavelength aperture is very important to be investigated.

Light transmission through a hole in an opaque screen has been studied for centuries. The well-known theoretical model, Bethe–Bouwkamp solution, has been proposed for analyzing the diffraction of electromagnetic radiation by a subwavelength circular hole in an infinitely thin and perfectly conducting screen [6,7]. Although a rigorous electromagnetic theory of diffraction by a circular aperture in a thick screen was developed, this method becomes numerically intractable for off-normal incidence [8]. In addition, to explain the experimental observation for the optical near-field of an aperture tip, another simple model was presented based on the assumption that the electric field produced by the tip is essentially static and is completely characterized by an assumed electric charge distribution [9–11].

More recently, the presence of tiny holes in an opaque metal film with sizes smaller than the wavelength of incident light has received growing attentions [12–15]. Due to the interaction of the light with electronic resonances on the surface of the metal film [16,17], subwavelength apertures in metal films can make the enhancement of the transmission magnitude by at most a factor of 7 [18,19]. This intriguing effect can be controlled by adjusting the size and geometry of the holes, as well as the thickness of the film [20].

For near-field optics, evanescent waves have to be taken into account because the energy exchange between the vibration surface and the electromagnetic wave at the near field prevents all the near-field energy to be transferred totally to the far field. The key concept of near-field optics involves evanescent electromagnetic waves, which makes it difficult to use any simple approximation in Maxwell's equations.

In this paper, near-field optical thin microcavity theory is proposed by applying the power flow theorem and the variable theorem, the electromagnetic field distribution inside and outside the thin microcacity can be obtained accurately and the thin microcavity theory is verified by comparing our results with those in the literatures. This paper is organized as follows: we derive the optical thin microcavity theory in details in Section 2. In Section 3, based on the thin microcavity theory, the near-field optical diffraction from a subwavelength aperture embedded in a perfect

* Corresponding author.
E-mail address: ejhwu@mail.xjtu.edu.cn (J.H. Wu).

http://dx.doi.org/10.1016/j.optcom.2015.09.029
0030-4018/

electrical conducting (PEC) thin film is investigated theoretically, and all the components are obtained accurately by using the Hankel transform. Further, the thin microcavity theory is verified in Section 4, followed by the conclusions in Section 5.

2. Thin microcavity theory

The governing equation of the electromagnetic field distribution in a thin microcavity under an external light incidence is derived in details. For a thin microcavity, we think it satisfies the condition that the thickness h is much less than the incident wavelength λ, i.e. $h \le (1/5\sim1/10)\lambda$. Because of the small thickness of the thin microcavity, we make the assumptions, as in Ref. [21], that the magnetic field component H_3 in the z direction, i.e., perpendicular to the symmetric plane of the microcavity with the origin at the center, is constant along the z direction, and the other components in x and y directions are $H_1 = z\partial H_3/\partial y$ and $H_2 = -z\partial H_3/\partial x$, respectively. The electromagnetic field components have the forms as following

$$\boldsymbol{H}(x, y, z) = [H_1(x, y, z), H_2(x, y, z), H_3(x, y)] \tag{1}$$

$$\boldsymbol{E}(x, y, z) = [E_1(x, y), E_2(x, y), E_3(x, y, z)] \tag{2}$$

Then the electric field components in the microcavity can be expressed as

$$\begin{aligned} -i\omega\varepsilon E_1 = \frac{\partial H_3}{\partial y} + \frac{\partial H_3}{\partial x}, -i\omega\varepsilon E_2 = \frac{\partial H_3}{\partial y} - \frac{\partial H_3}{\partial x}, -i\omega\varepsilon E_3 \\ = -z\frac{\partial^2 H_3}{\partial y^2} - z\frac{\partial^2 H_3}{\partial x^2} \end{aligned} \tag{3}$$

where the parameter ω is the circular frequency, ε is the permittivity of the microcavity material and i is the imaginary unit. It can be easily verified that $\nabla\cdot\boldsymbol{H} = 0$ and $\nabla\cdot\boldsymbol{E} = 0$, thus all Maxwell's equations are satisfied. Comparing Maxwell's equations $-i\omega\varepsilon E_1 = \partial H_3/\partial y - \partial H_2/\partial z$ and $-i\omega\varepsilon E_2 = \partial H_1/\partial z - \partial H_3/\partial x$ with Eq. (1), combining $H_1 = z\partial H_3/\partial y$ and $H_2 = -z\partial H_3/\partial x$, we can confirm the above assumptions, because $\partial H_2/\partial z \approx H_2/z$ and $\partial H_1/\partial z \approx H_1/z$ are both correct for small thickness.

The electric field energy U and the magnetic field energy T can be expressed as

$$\begin{aligned} U &= \int_V \frac{1}{2}\left(\varepsilon|\boldsymbol{E}|^2\right)dV = \frac{1}{2}\iint\int_{-h/2}^{h/2}\left(\varepsilon|\boldsymbol{E}|^2\right)dzdxdy \\ &= \frac{1}{2\omega^2\varepsilon}\iint\left\{2h\left[\left(\frac{\partial H_3}{\partial y}\right)^2 + \left(\frac{\partial H_3}{\partial x}\right)^2\right] + \frac{h^3}{12}\left(\frac{\partial^2 H_3}{\partial x^2} + \frac{\partial^2 H_3}{\partial y^2}\right)^2\right\}dxdy \end{aligned} \tag{4}$$

and

$$\begin{aligned} T &= \int_V \frac{1}{2}\left(\mu|\boldsymbol{H}|^2\right)dV = \frac{1}{2}\iint\int_{-h/2}^{h/2}\left(\mu|\boldsymbol{H}|^2\right)dzdxdy \\ &= \frac{\mu}{2}\iint\left\{\frac{h^3}{12}\left[\left(\frac{\partial H_3}{\partial y}\right)^2 + \left(\frac{\partial H_3}{\partial x}\right)^2\right] + hH_3{}^2\right\}dxdy \end{aligned} \tag{5}$$

where μ is the permeability and h is the thickness of the microcavity.

With an incident light, time-harmonic electromagnetic field of the thin microcavity satisfies the power flow theorem, the complex form of the power flow theorem can be expressed as

$$-\oint_s\left(\boldsymbol{E}\times\boldsymbol{H}^*\right)\cdot dS = i\omega\int_V\left(\boldsymbol{B}\cdot\boldsymbol{H}^* - \boldsymbol{E}\cdot\boldsymbol{D}^*\right)dV + \int_V \boldsymbol{E}\cdot\boldsymbol{J}^* dV \tag{6}$$

where $\boldsymbol{H}^*$, $\boldsymbol{D}^*$, $\boldsymbol{J}^*$ are the conjugate complex vectors of $\boldsymbol{H}$, $\boldsymbol{D}$, $\boldsymbol{J}$, respectively. Considering Eqs. (4) and (5), Eq. (6) can be written as

$$-\frac{1}{2i\omega}\oint_s\left(\boldsymbol{E}\times\boldsymbol{H}^*\right)\cdot dS = T - U \tag{7}$$

Due to the small thickness of the microcavity, we can ignore the surface integral term parallel to z direction. Thus, we can obtain that

$$\oint_S\left(\boldsymbol{E}\times\boldsymbol{H}^*\right)\cdot dS = \int_{S_1}\left(\boldsymbol{E}\times\boldsymbol{H}^*\right)\cdot dS + \int_{S_2}\left(\boldsymbol{E}\times\boldsymbol{H}^*\right)\cdot dS \tag{8}$$

where S_1 and S_2 indicate the upper and lower interface of the thin microcavity. It can be noticed that

$$\begin{aligned} \int_{S_1}\left(\boldsymbol{E}\times\boldsymbol{H}^*\right)\cdot dS &= \int_{S_1}\left(E_1H_2{}^* - E_2H_1{}^*\right)dS \\ &= -\int_{S_1}\left(\frac{h}{2}\frac{\partial H_3}{\partial x}E_1|_{z=\frac{h}{2}} + \frac{h}{2}\frac{\partial H_3}{\partial y}E_2|_{z=\frac{h}{2}}\right)dS \end{aligned} \tag{9}$$

and

$$\begin{aligned} \int_{S_2}\left(\boldsymbol{E}\times\boldsymbol{H}^*\right)\cdot dS &= \int_{S_2}\left(E_1H_2{}^* - E_2H_1{}^*\right)\cdot dS \\ &= -\int_{S_2}\left(\frac{h}{2}\frac{\partial H_3}{\partial x}E_1|_{z=-\frac{h}{2}} + \frac{h}{2}\frac{\partial H_3}{\partial y}E_2|_{z=-\frac{h}{2}}\right)dS \\ &= \int_{S_1}\left(\frac{h}{2}\frac{\partial H_3}{\partial x}E_1|_{z=-\frac{h}{2}} + \frac{h}{2}\frac{\partial H_3}{\partial y}E_2|_{z=-\frac{h}{2}}\right)dS \end{aligned} \tag{10}$$

Then Eq. (8) can be expressed as

$$\begin{aligned} -\oint_S\left(\boldsymbol{E}\times\boldsymbol{H}^*\right)\cdot dS &= -\int_{S_1}\left(\frac{h}{2}\frac{\partial H_3}{\partial x}E_1|_{z=\frac{h}{2}} + \frac{h}{2}\frac{\partial H_3}{\partial y}E_2|_{z=\frac{h}{2}}\right)dS + \\ &\int_{S_1}\left(\frac{h}{2}\frac{\partial H_3}{\partial x}E_1|_{z=-\frac{h}{2}} + \frac{h}{2}\frac{\partial H_3}{\partial y}E_2|_{z=-\frac{h}{2}}\right)dS \\ &= \frac{h}{2}\int_{S_1}\left[\frac{\partial H_3}{\partial x}\left(-E_1|_{z=\frac{h}{2}} + E_1|_{z=-\frac{h}{2}}\right) + \frac{\partial H_3}{\partial y}\left(-E_2|_{z=\frac{h}{2}} + E_2|_{z=-\frac{h}{2}}\right)\right]dS \end{aligned} \tag{11}$$

According to the variation of Eq. (7), and considering the arbitrariness of δH_3, the following governing equation for the time-harmonic magnetic field of the thin microcavity can be obtained that

$$\nabla^4 H_3 - k^4 H_3 = \frac{-3i\omega\varepsilon}{h^2}\left[\left.\frac{\partial E_{3U}}{\partial z}\right|_{z=h/2} - \left.\frac{\partial E_{3D}}{\partial z}\right|_{z=-h/2}\right] \tag{12}$$

where $\nabla^4 = \partial^4/\partial x^4 + 2\partial^4/(\partial x^2\partial y^2) + \partial^4/\partial y^4$, $k^4 = (\mu\varepsilon\omega^2h^2 - 12)\mu\varepsilon\omega^2/h^2$, k is the propagation constant in the microcavity. $E_{3U}(x, y, z)$ and $E_{3D}(x, y, z)$ are the electric field components in the z direction on both sides of the microcavity, the subscripts U and D denote the upper and lower spaces, respectively.This derived equation has an obvious physical meaning that the magnetic field distribution inside the microcavity is determined by the difference between the electric field gradients at the interfaces.

In the following, a special case will be further discussed. Without the incident light, Eq. (12) is then changed into the following equation for analyzing the resonant modes.

$$\nabla^4 H_3 - k^4 H_3 = 0 \tag{13}$$

In polar coordinates, the solution of Eq. (13) can be expressed as

$$H_3(r, \theta) = \sum_{n=0}^{\infty}\left[A_nJ_n(kr) + B_nY_n(kr) + C_nI_n(kr) + D_nK_n(kr)\right]\cos(n\theta) \tag{14}$$

where J_n and Y_n are the Bessel functions of the first and second kind, I_n and K_n are the modified Bessel functions of the first and second kind, respectively; the coefficients A_n, B_n, C_n and D_n can be

determined by the boundary conditions. Due to the properties of Y_n and K_n, there must be $B_n = 0$ and $D_n = 0$, because H_3 and $\partial H_3/\partial r$ at the center of the microcavity should be finite. Thus, we can obtain that

$$H_3(r, \theta) = \sum_{n=0}^{\infty} \left[A_n J_n(kr) + C_n I_n(kr)\right]\cos(n\theta) \tag{15}$$

For a solid microdisk with the radius $r = a$, the boundary conditions are $H_3|_{r=a} = 0$ and $\partial H_3/\partial r|_{r=a} = 0$, from which, we can obtain the following frequency equation

$$\det \begin{vmatrix} J_n(ka) & I_n(ka) \\ J_n'(ka) & I_n'(ka) \end{vmatrix} = 0 \tag{16}$$

For a rectangular microcavity with the sides of length a and b, H_3 can be expressed in Cartesian coordinates as

$$H_3(r, \theta) = \sum_{n=0}^{\infty} \left[A_n J_n\left(k\sqrt{x^2+y^2}\right) + C_n I_n\left(k\sqrt{x^2+y^2}\right)\right]\cos\left(n \tan^{-1}(y/x)\right) \tag{17}$$

which should accordingly satisfy the following boundary conditions

$$H_3|_{x=0,a} = 0, \quad \left.\frac{\partial H_3}{\partial x}\right|_{x=0,a} = 0,$$
$$H_3|_{y=0,b} = 0, \quad \left.\frac{\partial H_3}{\partial y}\right|_{y=0,b} = 0. \tag{18}$$

Considering the monotonically increasing property of $I_n(x)$ for any real number x, and $\lim_{n\to\infty} I_n(x) \to \infty$, we have to impose $C_n = 0$ for all resonant frequencies. In this case, Eq. (17) is the same as the exact solution of the 2D rectangular microcavity in appearance [22], but with a different wavenumber, because of the finite height. The resonant mode function for different orders (n, m) can be constructed as

$$\begin{aligned} H_3^{(n,m)} &= A_n\{J_{n-m}(kx) + J_{n-m}[k(a-x)] - J_{n-m}(ka) \\ &\quad - J_{n-m}(0)\} \\ &\{J_m(ky) + J_m[k(b-y)] - J_m(kb) - J_m(0)\} \\ &\cos(m\pi/2)\cos(n\pi/2) \end{aligned} \tag{19}$$

with the frequency equations

$$J_{n-m}'(ka) = 0, \quad J_m'(kb) = 0 \tag{20}$$

From the exact solutions of the governing equation and frequency equations, the resonant patterns of a thin microdisk and a thin rectangular microcavity can be obtained easily.

Based on the thin microcavity theory presented above, we further theoretically analyze near-field optical diffraction from a subwavelength aperture in a thin conducting film in the following.

3. Near-field optical diffraction from a subwavelength aperture in a thin conducting film

In this section, a near-field optical diffraction system that considers a perfect electrical conducting (PEC) thin film with a subwavelength aperture embedded will be investigated based on the thin microcavity theory. The sketch of the system is shown in Fig.1.

A plane wave vector $\boldsymbol{k_0}(k_0 = |\boldsymbol{k_0}| = 2\pi/\lambda)$ illuminates the system along the z axis. For simplicity the theory will be described for an E-polarized field incident upon the perfectly conducting metallic film. The incident electric field is given by $\boldsymbol{E_0} = E_0\boldsymbol{y} = \exp(ik_0 z)\boldsymbol{y}$, with the use of a time dependence in $\exp(-i\omega t)$. In Fig. 1, the reflected and transmitted field components in the upper (region I) and lower (region III) space can be expressed, respectively, as

$$\Phi^r(r, \theta, z) = \sum_{n=-\infty}^{\infty} \int_0^{\infty} \widetilde{\Phi}^r(\rho) J_n(\rho r) e^{i\sqrt{k_0^2-\rho^2}(z-h/2)} \rho d\rho e^{in\theta} \tag{21}$$

$$\Phi^t(r, \theta, z) = \sum_{n=-\infty}^{\infty} \int_0^{\infty} \widetilde{\Phi}^t(\rho) J_n(\rho r) e^{-i\sqrt{k_0^2-\rho^2}(z+h/2)} \rho d\rho e^{in\theta} \tag{22}$$

where J_n is the Bessel function of the first kind, $\widetilde{\Phi}^r(\rho)$ is the Hankel transform of $\Phi^r(r, 0, h/2)$ defined as $\widetilde{\Phi}^r(\rho) = \int_0^{\infty} \Phi^r(r, 0, h/2) J_n(\rho r) r dr$, and $\widetilde{\Phi}^t(\rho)$ is the Hankel transform of $\Phi^t(r, 0, -h/2)$ defined as $\widetilde{\Phi}^t(\rho) = \int_0^{\infty} \Phi^t(r, 0, -h/2) J_n(\rho r) r dr$. Here Φ^r represents for E_{1U}, E_{2U}, H_{1U} and H_{2U}, and Φ^t does for E_{1D}, E_{2D}, H_{1D} and H_{2D}. Eqs. (21) and (22) both satisfy the Helmholtz equation and include all the evanescent waves reflected and transmitted, respectively.

The magnetic field component H_3 in region II (vacuum) can be solved from Eq. (12) in a simple way as

$$H_3^d(r, \theta) = \sum_{n=0}^{\infty} \left[A_n J_n(kr) + C_n I_n(kr) + F_n \cdot r^n\right]\exp(in\theta) \tag{23}$$

where the coefficient A_n and C_n can be determined by the PEC boundary conditions $H_3^d(r, \theta)\big|_{r=a} = 0$ and $\partial/\partial r(r\partial H_3^d/\partial r)\big|_{r=a} = 0$, and $F_n \cdot r^n e^{in\theta}$ is the particular solution [23], the detailed derivation for F_n is shown later. The other electromagnetic components in the aperture, such as E_1^d, E_2^d, E_3^d, H_1^d, and H_2^d, can be also obtained from Eq. (23), which could solve the main drawback of the Bethe–Bouwkamp solution.

Because of the infinite PEC screen, the necessarily produced surface-current and charge densities are confined to the $z = \pm h/2$ planes. According to the reflection symmetries of the scattered fields [23], there are the following associated boundary conditions on surface of the film at $z = \pm h/2$

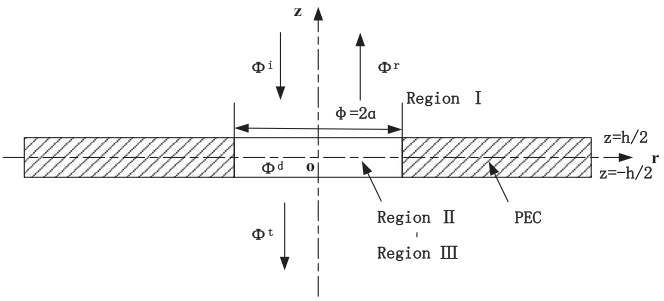

Fig. 1. Sketch of a thin film with a subwavelength aperture.

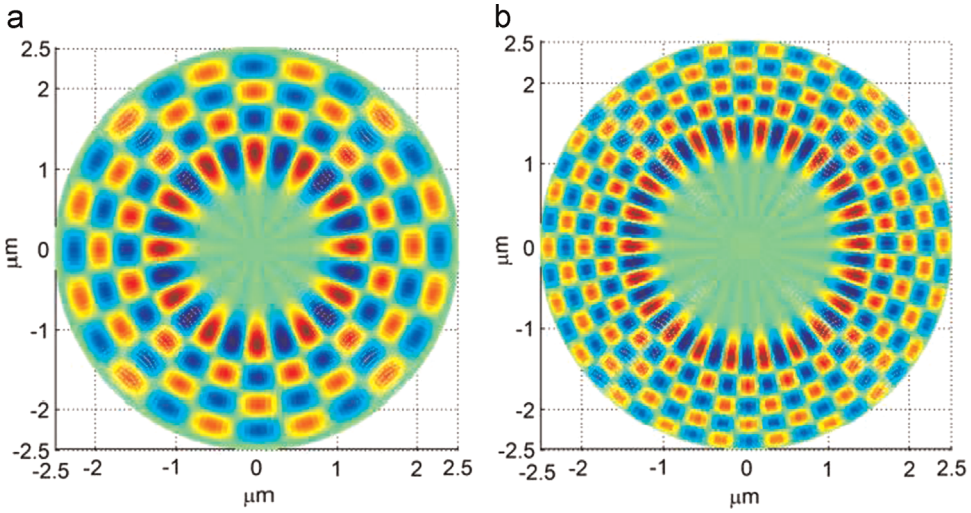

Fig. 2. Resonant patterns of a thin microdisk. (a) $n = 12$ and $ka = 42.22777$, (b) $n = 22$ and $ka = 51.7045$.

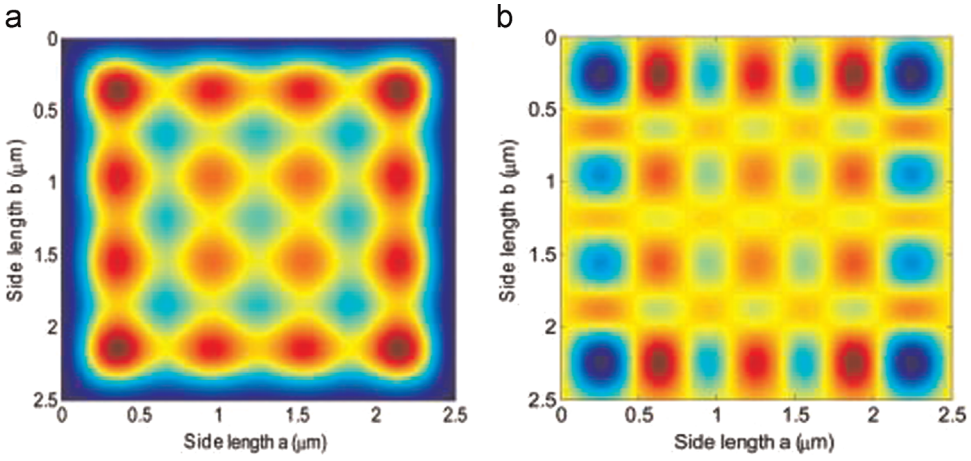

Fig. 3. Resonant patterns of mode numbers (n, m) of a square thin microcaivty. (a) $n = 0$, $m = 0$ and $ka = 38.47477$, (b) $n = 4$, $m = 2$ and $ka = 38.42265$.

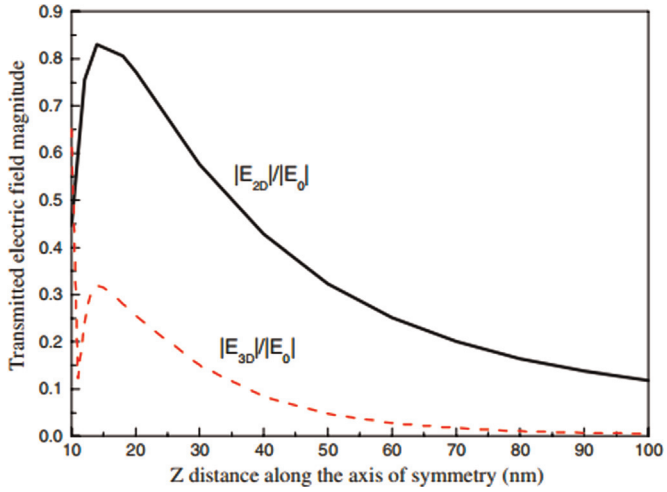

Fig. 4. Transmitted distance-dependent electric field magnitude along the axis of symmetry.

$$
\begin{aligned}
E_{1U}|_{z=h/2} &= E_{1D}|_{z=-h/2} = \begin{cases} E_1^d|_{z=h/2} & (r \le a) \\ 0 & (r > a) \end{cases}, \\
E_{2U}|_{z=h/2} &= E_{2D}|_{z=-h/2} = \begin{cases} E_2^d|_{z=h/2} & (r \le a) \\ -\exp(ik_0 h/2) & (r > a) \end{cases}, \\
H_{1U}|_{z=h/2} &= \begin{cases} H_1^d|_{z=h/2} & (r \le a) \\ -\dfrac{k_0}{\omega\mu}\exp(ik_0 h/2) & (r > a) \end{cases}, \\
H_{2U}|_{z=h/2} &= H_{2D}|_{z=-h/2} = \begin{cases} H_2^d|_{z=h/2} & (r \le a) \\ 0 & (r > a) \end{cases}, \\
H_{1D}|_{z=-h/2} &= \begin{cases} H_1^d|_{z=-h/2} = -H_1^d|_{z=h/2} & (r \le a) \\ \dfrac{k_0}{\omega\mu}\exp(ik_0 h/2) & (r > a) \end{cases},
\end{aligned}
\tag{24}
$$

Then the reflected and transmitted fields in region I and III can be obtained from (Eqs. (21) and 22) by use of the Hankel transform

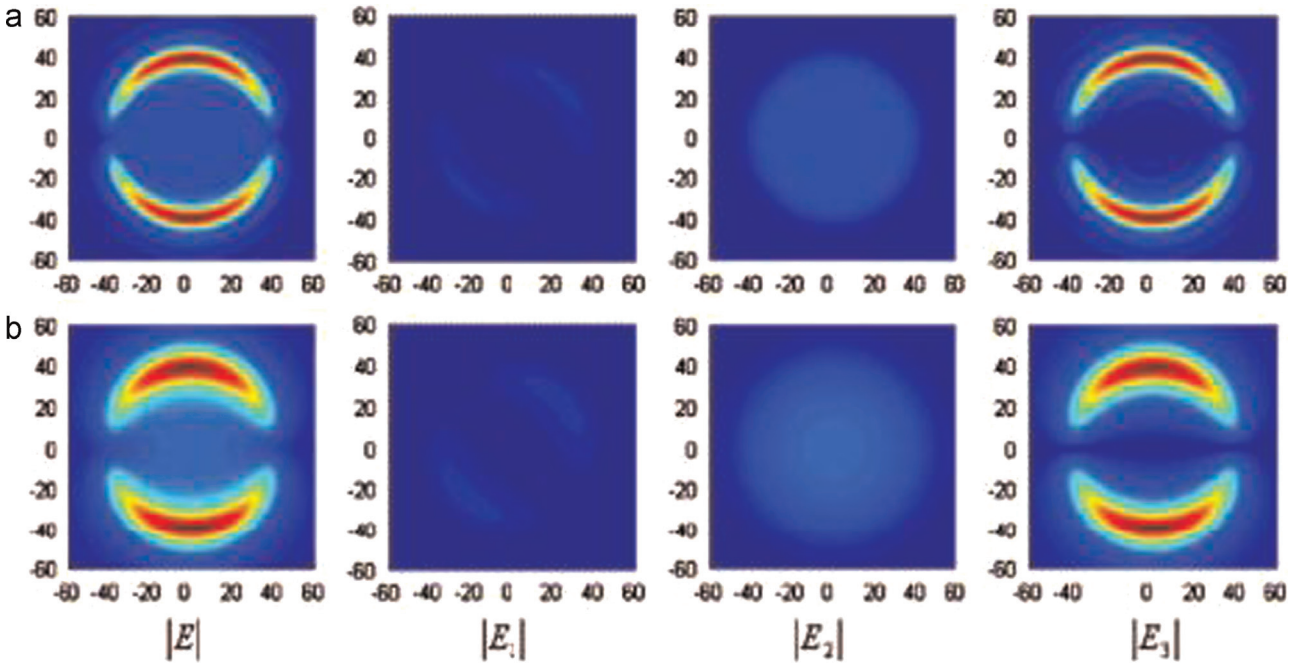

Fig. 5. Intensity maps for the electric field ($|E|$ and the components $|E_1|$, $|E_2|$, and $|E_3|$) created by the model presented at different cross sections; (a) $z_0 = -14$nm, (b) $z_0 = -18$nm. All image in each row share the same color bar. (For interpretation of the references to color in this figure legend, the reader is referred to the web version of this article.)

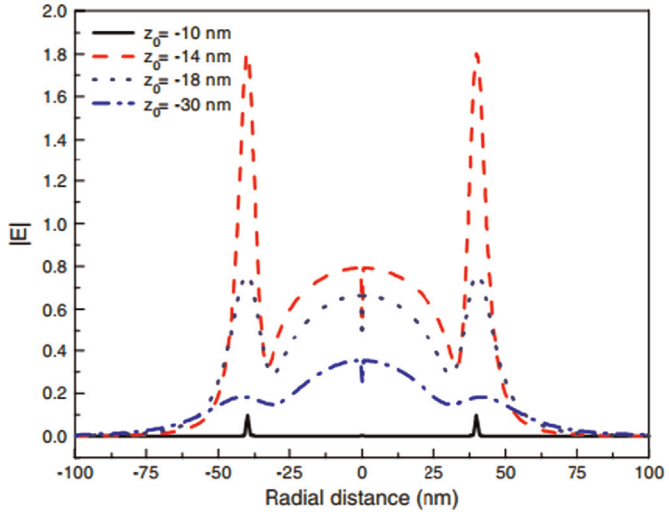

Fig. 6. Total electric field magnitude at the different observation points in the longitudinal section $y = 0$.

and continuous conditions of the tangential components at the interfaces.

In order to determine the coefficient F_n, we transform the right expression of Eq. (12) into the following by using the Maxwell's equation $\nabla \times H = i\omega\varepsilon E$

$$\nabla^4 H_3^d - k^4 H_3^d = \frac{3}{h^2}\left[\left(\frac{\partial^2 H_{2U}}{\partial x \partial z} - \frac{\partial^2 H_{1U}}{\partial y \partial z}\right)\Big|_{z=h/2} - \left(\frac{\partial^2 H_{2D}}{\partial x \partial z} - \frac{\partial^2 H_{1D}}{\partial y \partial z}\right)\Big|_{z=-h/2}\right] \tag{25}$$

According to Eqs. (21) and (22), all the right items of Eq. (25) can be expressed as

$$\begin{aligned}
\frac{\partial^2 H_{2U}}{\partial x \partial z}\Big|_{z=h/2} &= \sum_{n=-\infty}^{\infty} \int_0^{\infty} \widetilde{H}_{2U}(\rho) \frac{\partial J_n(\rho r)}{\partial x} i\sqrt{k_0^2 - \rho^2}\, \rho d\rho \\
&\quad e^{in\theta}, \\
\frac{\partial^2 H_{1U}}{\partial y \partial z}\Big|_{z=h/2} &= \sum_{n=-\infty}^{\infty} \int_0^{\infty} \widetilde{H}_{1U}(\rho) \frac{\partial J_n(\rho r)}{\partial y} i\sqrt{k_0^2 - \rho^2}\, \rho d\rho \\
&\quad e^{in\theta}, \\
\frac{\partial^2 H_{2D}}{\partial x \partial z}\Big|_{z=-h/2} &= \sum_{n=-\infty}^{\infty} \int_0^{\infty} \widetilde{H}_{2D}(\rho) \frac{\partial J_n(\rho r)}{\partial x} (-i) \\
&\quad \sqrt{k_0^2 - \rho^2}\, \rho d\rho e^{in\theta}, \\
\frac{\partial^2 H_{1D}}{\partial y \partial z}\Big|_{z=-h/2} &= \sum_{n=-\infty}^{\infty} \int_0^{\infty} \widetilde{H}_{1D}(\rho) \frac{\partial J_n(\rho r)}{\partial y} (-i) \\
&\quad \sqrt{k_0^2 - \rho^2}\, \rho d\rho e^{in\theta}
\end{aligned} \tag{26}$$

Then, substituting Eq. (26) into Eq. (25), after some manipulation, we can obtain that

$$\begin{aligned}
&\nabla^4 H_3^d - k^4 H_3^d = \frac{3}{h^2}\Bigg[\sum_{n=-\infty}^{\infty} \int_0^{\infty} \left(\widetilde{H}_{2U}(\rho) + \widetilde{H}_{2D}(\rho)\right) \frac{\partial J_n(\rho r)}{\partial x} i\sqrt{k_0^2 - \rho^2}\, \rho d\rho e^{in\theta} \\
&- \sum_{n=-\infty}^{\infty} \int_0^{\infty} \left(\widetilde{H}_{1U}(\rho) + \widetilde{H}_{1D}(\rho)\right) \frac{\partial J_n(\rho r)}{\partial y} i\sqrt{k_0^2 - \rho^2}\, \rho d\rho e^{in\theta}\Bigg]
\end{aligned} \tag{27}$$

According to Eq. (24), it can be derived that

$$\begin{aligned}
&\sum_{n=-\infty}^{\infty} \int_0^{\infty} \left(\widetilde{H}_{2U}(\rho) + \widetilde{H}_{2D}(\rho)\right) J_n(\rho r) \rho d\rho e^{in\theta} \\
&= H_{2U}(\rho, z)|_{z=h/2} + H_{2D}(\rho, z)|_{z=-h/2} = 0, \\
&\sum_{n=-\infty}^{\infty} \int_0^{\infty} \left(\widetilde{H}_{1U}(\rho) + \widetilde{H}_{1D}(\rho)\right) J_n(\rho r) \rho d\rho e^{in\theta} \\
&= H_{1U}(\rho, z)|_{z=h/2} + H_{1D}(\rho, z)|_{z=-h/2} = -H_{10}|_{z=h/2} \\
&= \frac{k_0}{\omega\mu} e^{ik_0 h/2} = \frac{k_0}{\omega\mu} e^{ik_0 h/2} \frac{1}{\pi i} \sum_{n=-\infty}^{\infty} \frac{1 - (-1)^n}{n} e^{in\theta}
\end{aligned} \tag{28}$$

Here note that the relation $1 = (1/\pi i)\sum_{n=-\infty}^{\infty}[1-(-1)^n]e^{in\theta}/n$ is used when the Eq. (28) is derived. Thus, we can yield

$$\widetilde{H}_{2U}(\rho) + \widetilde{H}_{2D}(\rho) = 0,$$

$$\widetilde{H}_{1U}(\rho) + \widetilde{H}_{1D}(\rho) = \begin{cases} \dfrac{k_0}{\omega\mu}e^{ik_0h/2}\dfrac{1}{\pi i}\dfrac{1-(-1)^n}{n}\dfrac{\delta(\rho)}{\rho^{n+1}}, & n \neq 0 \\ \dfrac{k_0}{\omega\mu}e^{ik_0h/2}\dfrac{1}{\pi i}\dfrac{1-(-1)^n}{n}\dfrac{\delta(\rho)}{\rho}, & n = 0 \end{cases} \tag{29}$$

Substituting Eq. (29) into Eq. (27), the governing equation becomes

$$\begin{aligned} &\nabla^4 H_3^d - k^4 H_3^d \\ &= -\frac{3}{h^2}\sum_{n=-\infty}^{\infty}\int_0^{\infty}\left(\widetilde{H}_{1U}(\rho)+\widetilde{H}_{1D}(\rho)\right)\frac{\partial J_n(\rho r)}{\partial y} i\sqrt{k_0^2-\rho^2}\,\rho d\rho e^{in\theta} \\ &= -\frac{3}{h^2}\sum_{n=-\infty}^{\infty}\int_0^{\infty}\frac{k_0}{\omega\mu}e^{ik_0h/2}\frac{1}{\pi i}\frac{1-(-1)^n}{n}\frac{\delta(\rho)}{\rho^{n+1}}\frac{\partial J_n(\rho r)}{\partial y} i \\ &\quad \sqrt{k_0^2-\rho^2}\,\rho d\rho e^{in\theta} \\ &= \frac{3}{2\pi h^2 i}\frac{k_0}{\omega\mu}e^{ik_0h/2}\sum_{n=0}^{\infty}\frac{1-(-1)^{n+1}}{n+1}\frac{r^n}{n!2^n}e^{in\theta} \end{aligned} \tag{30}$$

For a function $u = r^n e^{in\theta}$, we have

$$\nabla^4 u = \frac{\partial^4 u}{\partial r^4} + \frac{2}{r}\frac{\partial^3 u}{\partial r^3} - \frac{2n^2+1}{r^2}\frac{\partial^2 u}{\partial r^2} + \frac{2n^2+1}{r^3}\frac{\partial u}{\partial r} + \frac{n^4-4n^2}{r^4}u \tag{31}$$

By this formula, it can be found that $\nabla^4 u$ is identically equal to zero for any n. Thus, $\nabla^4 H_3 = 0$ is always correct for the particular solution. Then Eq. (30) can be changed into

$$-k^4 F_n = \frac{3}{2\pi h^2 i}\frac{k_0}{\omega\mu}e^{ik_0h/2}\frac{1-(-1)^{n+1}}{n+1}\frac{1}{n!2^n} \tag{32}$$

Then the coefficient F_n is easily obtained as

$$F_n = \frac{3k_0^2\exp(ik_0h/2)}{\pi h^2(i\omega\mu)k^4}\cdot\frac{(-1)^{n+1}-1}{(n+1)2^{n+1}n!} \tag{33}$$

4. Results and verification

According to the thin microcavity theory, we calculate the resonant patterns of a thin microdisk and a thin rectangular microcavity, and the transmitted field distribution of a subwavelength aperture embedded in a thin film under an incident light in the following.

Figs. 2 and 3 show the resonant patterns of a thin microdisk and a thin rectangular microcavity, respectively. The parameters of microdisk are: thickness $h = 0.2\mu$m, radius $a = 2.5\mu$m, and refractive index $n_e = 3.4$. In Fig. 2, the resonant pattern of the thin microdisk for the magnetic field component H_3 is axially symmetric, and is becoming more intensive when the mode order is increased from $n=12$ to $n=22$. The parameters of the rectangular microcavity are: thickness $h = 0.2\mu$m, length and width $a = b = 2.5\mu$m, and refractive index $n_e = 3.4$. In Fig. 3, the resonant pattern of mode numbers (n, m) of a square thin microcaivty for the magnetic field component H_3 is also symmetric, and is becoming more intensive when the mode numbers are increased from (0, 0) to (4, 2).

The results are in close agreement with the previous results in Ref. [24], in which the equivalent index, resonant wavelength and two-dimensional mode field distribution were approximately calculated by simultaneously solving guided-wave equation and axially symmetric wave equation with boundary conditions at disk center, edge and infinite distance. In compared with this method, our method is much simpler and more directly, but with the limitation of thin disks.

For the incident E-polarized plane wave $\boldsymbol{E_0} = E_0\boldsymbol{y} = \exp(ik_0z - i\omega t)\boldsymbol{y}$, by using the Hankel transform and boundary conditions at the interfaces presented above, we calculate the transmitted electric fields at different observation points (r_0, θ_0, z_0) with the following parameters: film thickness $h = 20$nm, radius of the aperture $a = 40$nm, and wavelength of the polarized incident plane wave $\lambda = 633$nm.

Fig. 4 displays the transmitted distance-dependent electric field magnitude along the axis of symmetry. Below the aperture, the electric field magnitude is polarization-dependent. E_{2D} is parallel to the incident field (p polarization), and there is a maximum value of $|E_{2D}|$ at $z_0 = -15$nm with monotonically decreasing there after. E_{3D} is vertical to the incident field (s polarization), and the field magnitude $|E_{3D}|$ is abrupt at the port interface $z_0 = -10$nm also with monotonically decreasing after a peak value at $z_0 = -14$nm. These polarization-dependent results are in very similar forms with the microwave measurement results in Ref. [25].

Fig. 5 shows the intensity distribution of the transmitted electric field, the total magnitude $|E| = \sqrt{|E_1|^2 + |E_2|^2 + |E_3|^2}$ and the components $|E_1|$, $|E_2|$ and $|E_3|$ at different cross sections, (a) $z_0 = -14$nm, (b) $z_0 = -18$nm. Due to the polarized incident wave, two intensity lobes along the aperture edge for the total electric field are produced. It can be observed that $|E|$ is entirely dominated by the y component $|E_2|$ and the z component $|E_3|$, and the x component $|E_1|$ can be ignored. $|E_2|$ is the highest in the image center where $|E_3|$ is negligible, while $|E_3|$ is the highest in the lobe centers where $|E_2|$ is very weak. The calculation results by the proposed thin microcavity theory are in good agreement with the experimental and simulation results for a near-field aperture tip in Ref. [9], which confirms that the thin microcavity theory can describe the near-field properties of NSOM. It also shows that the polarized incident light losts its polarization property after penetrating into the circular aperture, which is called the depolarization phenomenon. Because the polarized incident wave along the y direction is perpendicular to the hole edge, the abrupt change of the boundary conditions results in the discontinuity of the magnitude $|E|$ at the port interfaces and the depolarization of the electric field. Therefore, the depolarization phenomenon is a kind of edge effect, and the transmitted electric field shows a huge enhancement along the hole edge.

Fig. 6 shows the electric field magnitude $|E|$ at different distances $z_0 = -10$ nm, −14nm, −18nm, −30nm, respectively, in the longitudinal section $y = 0$. At the near field, the field magnitude is decreasing from the center to the hole edge, but abruptly increases when approaching the hole edge and to a huge maximum at the edge. On the other hand, this huge enhancement at the edge only exists in a certain range from the lower interface, since it is not obvious at $z_0 = -30$nm, Additionally, because $|E_3|$ is not continuous at the port interfaces, it is extremely small at $z_0 = -10$nm but much bigger at $z_0 = -14$nm, and then with the increase of the distance, the peak of the transmission through the subwavelength hole decreases rapidly, i.e. from 1.8 at $z_0 = -14$nm to 0.2 at $z_0 = -30$nm. The discontinuity of the field magnitude $|E|$ at the interfaces is due to the fact that the polarized incident wave along the y direction is perpendicular to the hole edge, and the abrupt change of the boundary conditions results in the depolarization of the electric field components and also the huge enhancement of the transmitted electric field along the hole edge. In addition, it is noted that the field magnitude has a sharp decrease

at the central point, which could be thought of as another kind of Poisson's spot. This phenomenon is very interesting and would be useful in trapping and manipulating photons, which will be investigated in detail later.

5. Conclusions

Near-field optical thin microcavity theory is presented here by applying the power flow theorem and the variable theorem, which is verified by the comparison between our results and those in the previous literatures. In the thin microcavity theory, the biharmonic differential governing equation of electromagnetic field can be solved exactly for a thin microcavity, and all the electromagnetic components, both inside and outside the microcavity, can be obtained accurately by using the Hankel transform. Moreover, based on the thin microcavity theory, the near-field optical diffraction from the subwavelength aperture embedded in the thin conducting film is investigated, in which the edge effect by an enhancement factor of 1.8 and the depolarization phenomenon of the transmission in terms of the distance from the film surface are discussed in details. These conclusions are interesting, and could find possible realistic applications in the future.

References

[1] L. Novotny, D.W. Pohl, B. Hecht, Scanning near-field optical probe with ultrasmall spot size, Opt. Lett. 20 (1995) 970–972.
[2] D.P. Tsai, W.C. Lin, Probing the near fields of the super-resolution near-field optical structure, Appl. Phys. Lett. 77 (2000) 1413–1415.
[3] P. Kramper, M. Kafasaki, C.M. Soukoulis, A. Birner, F. Müller, U. Gösele, R. B. Wehrspohn, J. Mlynek, V. Sandoghdar, Near-field visualization of light confinement in a photonic crystal microresonator, Opt. Lett. 29 (2004) 174–176.
[4] J.Y. Hsu, Nanolayer parametric instability in near-field optics, Opt. Lett. 29 (2004) 2157–2159.
[5] N. Louvion, A. Rahmani, C. Seassal, S. Callard, D. Gérard, F. de Fornel, Near-field observation of subwavelength confinement of photoluminescence by a photonic crystal microcavity, Opt. Lett. 31 (2006) 2160–2162.
[6] H.A. Bethe, Theory of diffraction by small holes, Phys. Rev. 66 (1944) 163–182.
[7] C.J. Bouwkamp, Diffraction theory, Rep. Prog. Phys. 17 (1954) 35–100.
[8] A. Roberts, Electromagnetic theory of diffraction by a circular aperture in a thick, perfectly conducting screen, J. Opt. Soc. Am. A4 (1987) 1970–1983.
[9] A. Drezet, M.J. Nasse, S. Huant, J.C. Woehl, The optical near-field of an aperture tip, Europhys. Lett. 66 (2004) 41–47.
[10] F.J. García de Abajo, Light transmission through a single cylindrical hole in a metallic film, Opt. Express 10 (2004) 1475–1484.
[11] C.W. Chang, A.K. Sarychev, V.M. Shalaev, Light diffraction by a subwavelength circular aperture, Laser Phys. Lett. 2 (2005) 351–355.
[12] H.J. Lezec, A. Degiron, E. Devaux, R.A. Linke, L. Martin-Moreno, F.J. Garcia-Vidal, T.W. Ebbesen, Beaming light from a subwavelength aperture, Science 297 (2002) 820–822.
[13] C. Genet, T.W. Ebbesen, Light in tiny holes, Nature 445 (2007) 39–46.
[14] R.L. Chern, C.Y. Kuo, H.W. Chen, C.C. Chang, Electromagnetic scattering by a subwavelength circular hole in a perfect metal plate of finite thickness: matched asymptotic expansion, J. Opt. Soc. Am. B27 (2010) 1031–1043.
[15] J. Jung, O. Keller, Microscope theory of diffraction of light from a small hole, Phys. Rev. A90 (2014) 043830.
[16] J. Fiala, I. Richter, Interaction of light with subwavelength apertures: a comparison of approximate and rigorous approaches, Opt. Quantum Electron. 41 (2009) 409–427.
[17] T. Thio, K.M. Pellerin, R.A. Linke, H.J. Lezec, T.W. Ebbesen, Enhanced light transmission through a single subwavelength aperture, Opt. Lett. 26 (2001) 1972–1974.
[18] T.W. Ebbesen, H.J. Lezec, H.F. Ghaemi, T. Thio, P.A. Wolff, Extraordinary optical transmission through sub-wavelength hole arrays, Nature 391 (1998) 667–669.
[19] H.J. Lezec, T. Thio, Diffracted evanescent wave model for enhanced and suppressed optical transmission through subwavelength hole arrays, Opt. Express 12 (2004) 3629–3651.
[20] S. Carretero-Palacios, F.J. García-Vidal, L. Martín-Moreno, Sergio G. Rodrigo, Effect of film thickness and dielectric environment on optical transmission through subwavelength holes, Phys. Rev. B85 (2012) 035417.
[21] J.H. Wu, A.Q. Liu, H.H. Li, Investigation of resonant modes in thin microcavities by using electromagnetic theory, Opt. Lett. 31 (2006) 2438–2440.
[22] J.H. Wu, A.Q. Liu, Exact solution of resonant modes in a rectangular resonator, Opt. Lett. 31 (2006) 1720–1722.
[23] J.H. Wu, Modeling of near-field optical diffraction from a subwavelength aperture in a thin conducting film, Opt. Lett. 36 (2011) 3440–3442.
[24] T. Baba, Photonic crystals and microdisk cavities based on GaInAsP–InP system, IEEE J. Sel. Top. Quantum Electron. 3 (1997) 808–830.
[25] G. Ctistis, O. Schimek, P. Fumagalli, J.J. Paggel, Polarization-dependent measurement of the near-field distribution of a waveguide with subwavelength aperture, J. Appl. Phys. 99 (2006) 014505.